Photodisintegration of ^{9}Be through the $1/2^{+}$ state and cluster dipole resonance

H. Utsunomiya,[1,2] S. Katayama,[1] I. Gheorghe,[3,4] S. Imai,[1] H. Yamaguchi,[2] D. Kahl,[2] Y. Sakaguchi,[2] T. Shima,[5] K. Takahisa,[5] and S. Miyamoto[6]

[1]*Department of Physics, Konan University, Okamoto 8-9-1, Higashinada, Kobe 658-8501, Japan*
[2]*Center for Nuclear Study, University of Tokyo, Hirosawa 2-1, Wako, Saitama 351-0198, Japan*
[3]*ELI-NP, "Horia Hulubei" National Institute for Physics and Nuclear Engineering (IFIN-HH), 30 Reactorului, 077125 Bucharest-Magurele, Romania*
[4]*Faculty of Physics, University of Bucharest, RO-077125 Bucharest, Romania*
[5]*Research Center for Nuclear Physics, Osaka University, Suita, Osaka 567-0047, Japan*
[6]*Laboratory of Advanced Science and Technology for Industry, University of Hyogo, 3-1-2 Kouto, Kamigori, Ako-gun, Hyogo 678-1205, Japan*

(Received 5 November 2015; published 29 December 2015)

Photodisintegration of ^{9}Be through the $1/2^{+}$ state near neutron threshold and cluster dipole resonance below giant dipole resonance was measured with quasi-monochromatic γ-ray beams produced in the inverse Compton scattering of laser photons. The cross section for the $1/2^{+}$ state is revisited, being consistent with the 2001 data. The cross section for the cluster dipole resonance is consistent with the cluster dipole sum-rule which however degenerates for the two-body (n-^{8}Be) and three-body(n-α-α) configurations.

DOI: 10.1103/PhysRevC.92.064323 PACS number(s): 25.20.Lj, 24.30.Gd, 27.20.+n

I. INTRODUCTION

Photodisintegration of ^{9}Be has drawn a renewed attention from the viewpoints of explosive nucleosynthesis of ^{9}Be and nuclear structure of the Borromean system. The nucleosynthesis of ^{9}Be may proceed through $\alpha + \alpha \rightleftharpoons {}^{8}$Be and ^{8}Be$(n, \gamma)^{9}$Be reaction [1] in astrophysical sites like Type-II supernovae [2] or neutron star mergers [3]. The explosive synthesis of ^{9}Be followed by ^{9}Be$(\alpha,n)^{12}$C may dominate over the triple α reaction to bridge the mass gaps at $A = 5$ and $A = 8$ [4]. Obviously, the ^{8}Be$(n,\gamma)^{9}$Be reaction cannot be investigated in the experimental laboratory because ^{8}Be is unstable. In contrast, the inverse photodisintegration of ^{9}Be is experimentally feasible and straightforward. Previously two experiments were performed to measure the photodisintegration cross section using quasi-monochromatic γ-ray beams produced in the inverse Compton scattering of laser photons with relativistic electrons [5,6]. The discrepancy between the two measurements is significant for the $1/2^{+}$ state near the n-^{8}Be threshold.

The big-bang nucleosynthesis of ^{9}Be may be catalyzed by a hypothetical long-lived negatively charged massive ($\gtrsim$100 GeV) leptonic particle, X^{-}, through the two-step resonant reaction $(^{8}\mathrm{Be}X^{-})_{\mathrm{atom}} + n \rightarrow (^{9}\mathrm{Be}_{\frac{1}{2}^{+}}X^{-})_{\mathrm{atom}} \rightarrow {}^{9}\mathrm{Be}_{\frac{3}{2}^{-}} + X^{-}$ [7]. A candidate for X^{-} is the supersymmetric (SUSY) counterpart of the tau lepton (τ), i.e., the stau ($\tilde{\tau}$) [8]. The observational upper limit in old stars, ^{9}Be/H $\leqslant 2.1 \times 10^{-13}$, may impose a strong constraint on the lifetime of X^{-}. It is however pointed out [9] that accurate information of the excitation energy of $^{9}\mathrm{Be}^{+}_{\frac{1}{2}}$ as well as the charge radius of ^{8}Be is required to calculate the reaction rate that is strongly affected by the resonance position of $(^{9}\mathrm{Be}_{\frac{1}{2}^{+}}X^{-})_{\mathrm{atom}}$ with respect to the $(^{8}\mathrm{Be}X^{-})_{\mathrm{atom}} + n$ threshold.

Besides its astrophysical significance, the $1/2^{+}$ state has raised an important question about the nuclear structure of ^{9}Be in terms of resonant state [10–12] or virtual [13–15] state. The threshold behavior of the $1/2^{+}$ state cross section may be attributed to a virtual state that is defined as a pole of the n-^{8}Be scattering matrix at the complex wave number $k = -i\kappa$ ($\kappa > 0$) as well as a resonant state at $k = k_1 - ik_2$ ($k_1 > k_2 > 0$).

An enhancement in photoneutron emission was reported for ^{9}Be in the energy region of 5–17 MeV immediately below the giant-dipole resonance (GDR) in the experiment with bremsstrahlung [16]. We hereby refer to the enhanced cross section as cluster dipole resonance (CDR) as we discuss in terms of the cluster dipole sum rule in Sec. IV. An experimental confirmation of the cross section is desirable to investigate the nuclear structure of CDR in the Borromean nucleus with a weakly bound neutron.

In this paper, we present experimental data for photodisintegration of ^{9}Be through the $1/2^{+}$ state and CDR.

II. EXPERIMENTAL PROCEDURE

We investigated photodisintegration of ^{9}Be through the $1/2^{+}$ state and CDR at the NewSUBARU synchrotron radiation facility. Quasi-monochromatic γ-ray beams were produced by the Compton backscattering between laser photons with 100% linear polarization and relativistic electrons in a head-on collision geometry [17]. The laser Compton scattering (LCS) γ-ray beam produced in the head-on collision is also linearly polarized nearly 100%. We present here details of the experiment with emphasis on the characteristics of the LCS γ-ray beam and the neutron detection.

A. Gamma beam production and energy profile

The γ-ray production beam line BL01 is shown in Fig. 1. Low- and high-energy γ-ray beams were produced using a grating-fixed CW CO_2 laser ($\lambda = 10.5915\,\mu$m ± 3 Å and a Q-switch Nd:YVO_4 INAZUMA laser ($\lambda = 1064$ nm), respectively. The nominal value of the electron beam energy was changed from 974 to 954 MeV in the decelerate mode of the storage ring and from 974 to 1121 MeV in the acceleration mode for low-energy γ production, while it was changed from

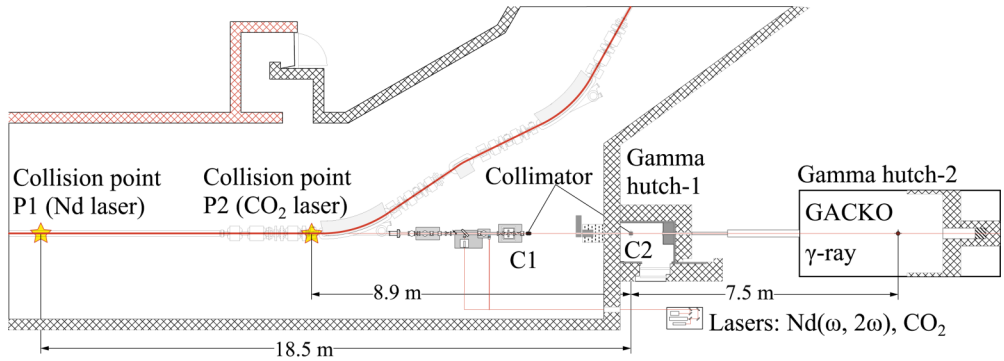

FIG. 1. (Color online) The γ-ray production beam line at the NewSUBARU synchrotron radiation facility.

974 to 962 MeV for the high-energy γ production. The beam line has two collision points, P1 for the Nd:YVO_4 laser and P2 for the CO_2 laser, located at 18.5 m and 8.9 m from a collimator C2 mounted in the Hutch 1. We used a 1 mm-diameter C2 collimator to produce low-energy γ-ray beams and a 2 mm-diameter C2 collimator to produce high-energy beams. In addition to the C2 collimator, a 3 mm-diameter C1 collimator was mounted in the storage-ring vault. All collimators are made of 10 cm-thick Pb.

Low-energy LCS γ-ray beams were measured with a high-purity Ge detector to determine the energy profile of the γ-ray beam, while high-energy γ-ray beams with a 3.5 in. $\times$ 4.0 in. $LaBr_3$(Ce) detector. The Ge crystal of 64.3 mm diameter and 60.1 mm length was irradiated 15 mm off the center to avoid the central hole for the inner electrode and cooling rod.

Figure 2 shows an example of response function of the Ge detector to a low-energy LCS γ-ray beam. The Ge detector was calibrated with the standard γ-ray sources (^{133}Ba, ^{137}Cs, and ^{60}Co including the sum peak). The full-energy peak is characterized by a high-energy edge and a low-energy tail. The edge slightly slopes, reflecting the energy resolutions of the electron beam ($\sim 4 \times 10^{-4}$) and the Ge detector. The energy spread of the tail reflects the kinematics of the Compton backscattering between laser photons and relativistic electrons into an aperture of the collimator. Monte Carlo simulations with the GEANT4 code [18] were carried out to reproduce the response function. The electron beam emittance, the double collimators, and the off-center irradiation of the Ge crystal were incorporated into the simulation. The response function (solid line) was well reproduced by the simulation (dotted line). By turning off the interaction of γ rays with the detector material (Ge) in the simulation code, we obtained an energy spectrum of the LCS γ-ray beam produced. The spectrum is shown by the grey line in Fig. 2. The energy spread of the low-energy γ-ray beams used for the study of the $1/2^+$ state was 1.8–3.5% in full width at half-maximum (FWHM).

Figure 3 shows an example of response function of the $LaBr_3$(Ce) detector to a high-energy LCS γ-ray beam. The energy calibration of the high-energy LCS γ-ray beams relied on the absolute calibration of the electron beam energies with the accuracy on the order of 10^{-5} [19]. The full-energy peak is visible for the 5.5 MeV γ-ray beam. Again the response function was well reproduced by the simulation. The energy spread of the high-energy γ-ray beams used for the study of the CDR was 1.4–2.2% in FWHM.

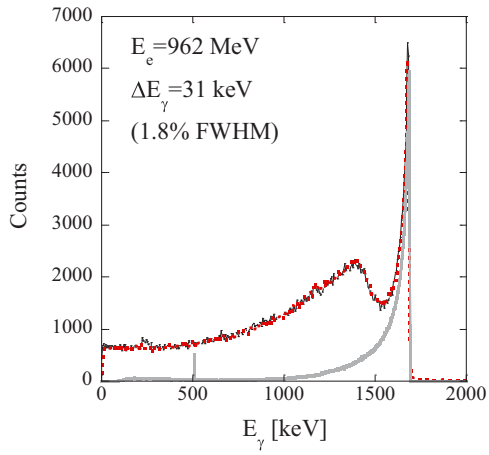

FIG. 2. (Color online) An experimental response function (solid line) of the Ge detector to a low-energy LCS γ-ray beam produced with the CO_2 laser along with the simulated response function (dotted line) and energy distribution of the LCS γ-ray beam (grey line).

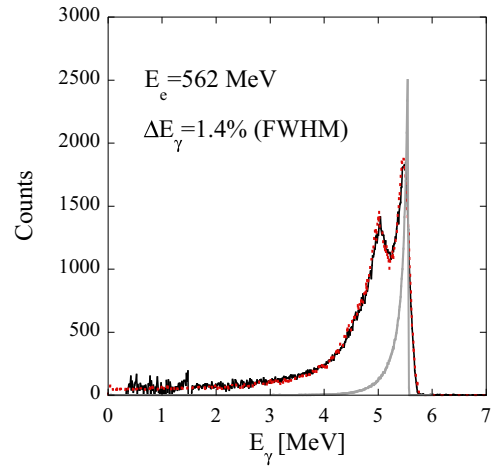

FIG. 3. (Color online) An experimental response function (solid line) of the $LaBr_3$(Ce) detector to a high-energy LCS γ-ray beam produced with the Nd:YVO_4 laser along with the simulated response function (dotted line) and energy distribution of the LCS γ-ray beam (grey line).

The intensity distribution of the LCS γ-ray beam at the target position was simulated with the GEANT4 code. With the 2 mm C2 collimator, the beam size on target was 2.3 mm in diameter in FWHM of the intensity distribution.

B. Target

A 99% ^{9}Be rod of 25 mm diameter and 40 mm length was used as a target. A natural carbon rod of the same dimension was also used to investigate the scattering effect of the LCS γ-ray beam [6]. No scattering effects were found compared with blank target runs. Heavy water (99.9%) in an aluminum container with entrance and exit windows of 25.4 μm-thick Kapton foil was used as a D_2O target of 14 mm diameter and 100 mm length. Photodisintegration of deuterium was measured at the electron beam energy 1460 MeV for a crosscheck of the present absolute cross section measurement. An empty target run confirmed a negligible effect of the Kapton foils on photoneutron emission.

C. γ-ray flux

A 8 in. $\times$ 12 in. NaI(Tl) detector with 100% detection efficiency was used as a γ-ray flux monitor. The flux determination is straightforward for LCS γ-ray beams produced with the CW CO_2 laser. The γ rays were detected with the NaI(Tl) detector at the count rate of 15–41 kcps. Energy spectra were recorded with a multichannel analyzer with a conversion time of $\sim$2.6 μs. The flux was determined by subtracting background γ rays and correcting for a small amount of double photon events.

The flux determination for pulsed LCS γ-ray beams produced with the Q-switch Nd:YVO_4 laser followed the Poisson-fitting method [20,21]. The laser was operated at 20 kHz. Laser photons with a pulse width 60 ns collide with relativistic electrons in the NewSUBARU storage ring at 500 MHz with a 20 ps pulse width. Although the number of pairs of laser photons and electrons involved in the collision during the 60 ns laser pulse (N) is large, the collision probability per photon-electron pair (p) is small. As a result, the number of collisions (n) is small with the average number $m = pN$. Under this condition, the distribution of the number of collision, $P_m(n)$, can be expressed by the Poisson distribution, $P_m(n) = \frac{m^n}{n} e^{-m}$. Multiphoton spectra generated by pulsed γ-ray beams measured with a NaI(Tl) were investigated at different γ-ray beam intensities and indeed characterized by the Poisson distribution [22]. Figure 4 shows a typical single- and multiphoton spectra. The number of γ rays (N_γ) is determined by $N_\gamma = mN_p$ with the average number of γ rays per γ pulse and the number of γ pulses, N_p. The N_p is equal to the number of total events of the multiphoton spectrum which is often referred to as pile-up spectrum. Empirically, the average number of γ rays per pulse m is given by the ratio of the average channel number of the multiphoton spectrum $[CH]_p^{av}$ to that of the single-photon spectrum $[CH]_s^{av}$, $m = \frac{[CH]_p^{av}}{[CH]_s^{av}}$ [22]. The uncertainty of the flux determination comes from the energy linearity in the response of the flux monitor detector to multiphotons. The uncertainty was estimated to be $\sim$3% [22].

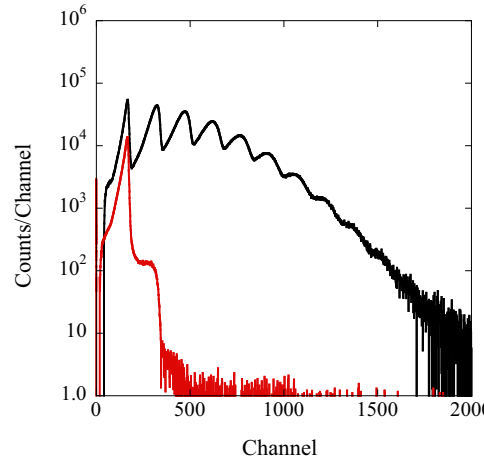

FIG. 4. (Color online) Multiphoton and single-photon spectra of the LCS γ-ray beam measured with the NaI(Tl) detector.

D. Neutron detection

Photoneutrons were detected with a 4π neutron detector composed of 20 ^{3}He proportional counters embedded in a polyethylene moderator in a triple-ring configuration. The concentric Ring-1 (R1), Ring-2 (R2), and Ring-3 (R3) of four, eight, and eight ^{3}He counters are placed at the distances of 38, 70, and 100 mm from the beam axis, respectively. This detector is designed with the MCNP code [23] for a highest total efficiency being more than 60% for neutrons below 1 MeV. Figure 5 shows detection efficiencies of Ring-1, Ring-2, and Ring-3 as well as the sum efficiency for isotropically emitted neutrons. The efficiencies were calibrated with a ^{252}Cf source at the National Metrology Institute of Japan (NMIJ). The detector has long been used for (γ, n) cross section measurements for heavy nuclei (see [24,25]

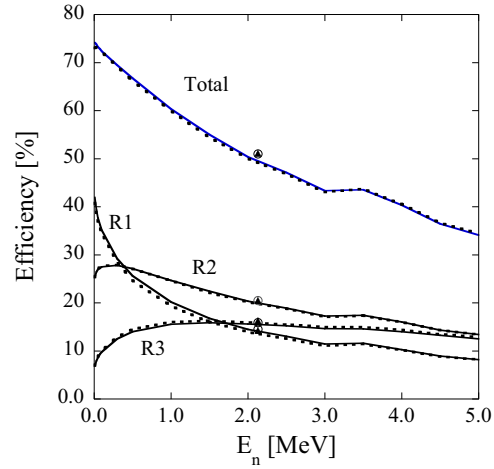

FIG. 5. (Color online) The detection efficiencies of the Ring-1, Ring-2, and Ring-3 and the total efficiency for s-wave (solid line) and p-wave (dotted lines) neutrons obtain by the GEANT4 simulation. The efficiencies measured with a calibrated ^{252}Cf source are shown by the solid triangles and those simulated with the MCNP Monte Carlo code are shown by the open circles.

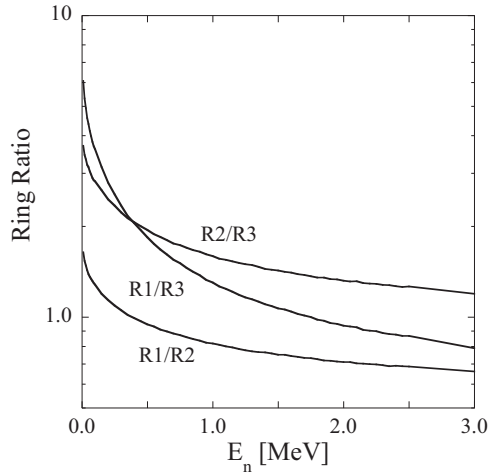

FIG. 6. The ring ratios of the present 4π neutron detector with Ring-1, Ring-2, and Ring-3 of four, eight, and eight ^{3}He counters embedded in a polyethylene moderator.

for the latest measurements and references therein). The detection efficiencies were recalibrated in advance to the present experiment using a ^{252}Cf source at a neutron emission rate 2.27×10^4 s^{-1} with 2.2% uncertainty at the NMIJ. The experimental calibration points were excellently reproduced.

There are two dominating modes of s-wave and p-wave photoneutron emissions. Besides the isotropic emission of s-wave neutrons, the detection efficiencies were also simulated for p-wave neutrons with the angular distribution $W_{\rm pol}(\theta,\phi) = \frac{3}{8\pi}[\sin^2\theta(1+\cos 2\phi)]$, where θ stands for the polar angle for photoneutron emission with respect to the beam direction (z axis), while ϕ for the azimuthal angle with respect to the linear polarization (x axis) of the γ-ray beam defined by a direction of the electric field. The results are shown in Fig. 5. One can see that Ring-1, Ring-2, and Ring-3 summed over four, eight, and eight ^{3}He counters, respectively, have the same efficiencies as for s- and p-wave neutrons. The angular distribution of p-wave neutrons is largely smeared out in the polyethylene moderator.

Figure 6 shows ratios of the detection efficiencies of Ring-1, Ring-2, and Ring-3 as a function of the neutron energy. The ring-ratio technique [26] which takes advantage of these unique energy dependences was used to determine the mean energy of neutrons emitted in each γ-ray beam irradiation; the neutron energies determined with the three ring ratios were weight-averaged. The weighted average was in turn used to determine the total detection efficiency of the 4π neutron detector. The mean neutron energy changed from 16 keV to 200 keV in the photodisintegration of ^{9}Be through the $1/2^+$ state, while it changed from 1.15 MeV to 1.99 MeV in the photodisintegration through CDR.

III. DATA REDUCTION

The experimental formula of photoneutron cross section is given by

$$\int_{S_n}^{E_{\rm max}} n_\gamma(E_\gamma)\sigma(E_\gamma)dE_\gamma = \frac{N_n}{N_t N_\gamma \xi \epsilon_n g}, \qquad (1)$$

where S_n is the neutron threshold energy, $E_{\rm max}$ is the maximum energy of the LCS γ-ray beam, $n_\gamma(E_\gamma)$ gives the energy distribution of the γ-ray beam normalized to unity and $\sigma(E_\gamma)$ is the photoneutron cross section to be determined. Furthermore, N_n represents the number of neutrons detected, N_t gives the number of target nuclei per unit area, N_γ is the number of γ rays incident on target, ϵ_n represents the neutron detection efficiency, and finally $\xi = (1-e^{\mu t})/(\mu t)$ gives a correction factor for a thick target measurement. The factor g represents a fraction of the γ flux above S_n.

The monochromatic cross section results when the $n(E_\gamma)$ in Eq. (1) is replaced by a δ function, $\delta(E_\gamma - E_0)$:

$$\sigma^{\rm mon}(E_0) = \frac{N_n}{N_t N_\gamma \xi \epsilon_n g}. \qquad (2)$$

There are two methods for deconvoluting the integral of Eq. (1) to obtain $\sigma(E_\gamma)$, the Taylor expansion method [24] and the least-squares method [27]. We summarize the Taylor expansion method which has long been used in (γ, n) cross section measurements for heavy nuclei (see [24] and references therein).

A deconvolution can be done by expanding $\sigma(E_\gamma)$ in the Taylor series at the average energy $E_{\rm av}$:

$$\sigma(E_\gamma) = \frac{1}{n!}\sum_{n=0}^{\infty}\sigma^{(n)}(E_{\rm av})(E_\gamma - E_{\rm av})^n. \qquad (3)$$

Putting Eq. (3) into Eq. (1), one obtains

$$\sigma(E_{\rm av}) = \sigma^{\rm mon}(E_{\rm av}) - s_2(E_{\rm av}) - s_3(E_{\rm av}) - \cdots, \qquad (4)$$

where

$$s_n(E_{\rm av}) = \frac{1}{n!}\sigma^{(n)}(E_{\rm av})\int_{S_n}^{E_{\rm max}} n_\gamma(E_\gamma)(E_\gamma - E_{\rm av})^n dE_\gamma \qquad (5)$$

and

$$\sigma^{(n)}(E_{\rm av}) = \left.\frac{d^n\sigma(E)}{dE^n}\right|_{E=E_{\rm av}}. \qquad (6)$$

Note that s_1 is zero by the definition of $E_{\rm av}$.

Since $\sigma^{(i)}(E_{\rm av})$ cannot be calculated until $\sigma(E_\gamma)$ is determined, an iteration procedure must be employed. The iteration begins with a best fit to the monochromatic cross section with an appropriate function and ends with a reasonable conversion. In the present data reduction, we used the Breit-Wigner formula for the $1/2^+$ data and a Lorentzian function for a specific fit to the CDR data. We approximate the best-fit function with the third-order polynomial in small energy bins to terminate the Taylor expansion at s_3 in Eq. (4).

The systematic uncertainty is estimated to be 4.4% which is a quadratic sum of 3% for the number of incident photons and 3.2% for the neutron detection efficiency.

IV. RESULTS AND DISCUSSIONS

A. Crosscheck with the D(γ,n)p cross section

The result of the present measurement of the D(γ,n)p reaction cross section is shown in Fig. 7. The present result is in good agreement with the existing data [28–32] and the JENDL evaluation [33].

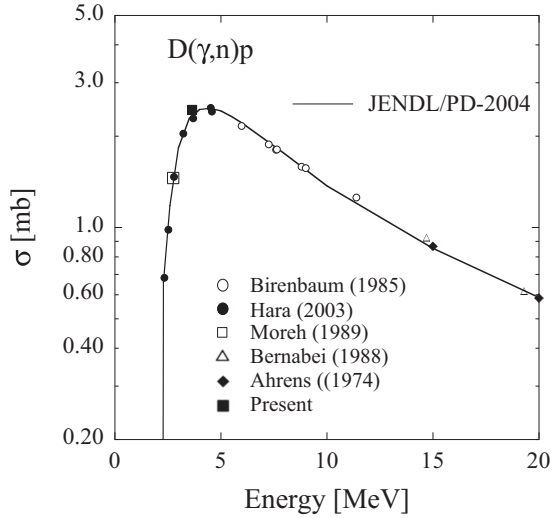

FIG. 7. The D(γ,n) cross section. The present datum is shown by the solid square.

The same LCS γ-ray beam was also used to measure the photodisintegration cross section for ^{9}Be. The result is shown by the thick open cross in Fig. 8 in comparison with the 2001 data (filled circles) [5] and 2012 data (open circles) [6]. The bremsstrahlung data (crosses) [16] are also shown in the figure. The 2012 data are the monochromatic cross sections retrieved from the EXFOR database [34]. We remark that the 2001 data were published in such a way that cross sections are plotted at the peak energies of the γ-ray beams with the horizontal error bars representing energy spreads of the beams in FWHM.

B. $1/2^+$ state

The mean neutron energy, $E_n^{\rm av}$, determined with the ring ratio technique is shown in Fig. 9 as a function of the γ-ray energy. The mean neutron energies near the n-^{8}Be threshold are consistent with the kinematics of two-body breakup $^9\mathrm{Be} \rightarrow n + {}^8\mathrm{Be}$, $E_n = \frac{8}{9}(E_\gamma - S_n)$. However, the $E_n^{\rm av}$ deviates from the two-body kinematics at the three

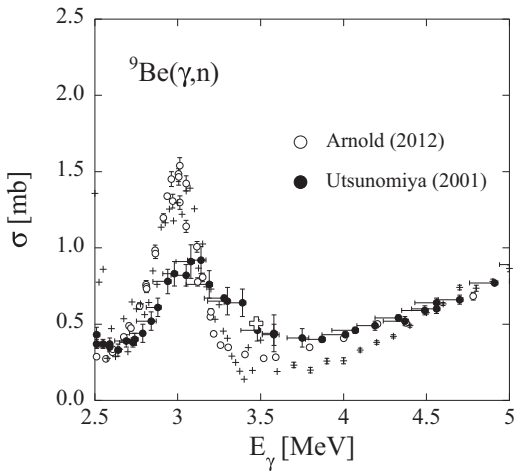

FIG. 8. The ^{9}Be(γ,n) cross section. The present datum is shown by the thick open cross.

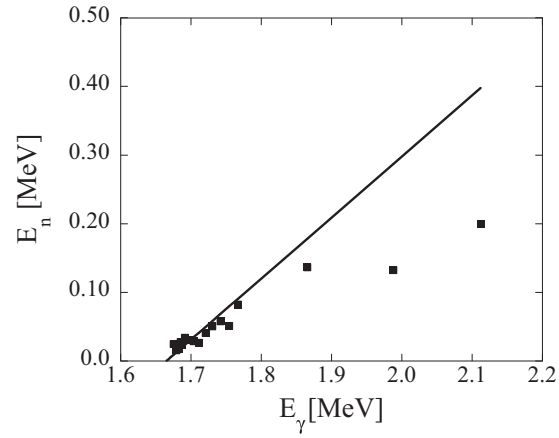

FIG. 9. The mean neutron kinetic energies determined by the ring ratio technique [26]. The two-body kinematics is shown by the solid line.

energies above 1.8 MeV. The deviation indicates the onset of three-body breakup, $^9\mathrm{Be} \rightarrow n + \alpha + \alpha$, in this energy region.

Figure 10 shows the present cross section for the $1/2^+$ state by the solid squares. The data were corrected for energy spreads of the LCS γ-ray beam with the Taylor expansion method. The monochromatic cross section is also shown by the open circles in the figure. The present measurement between the n-^{8}Be threshold at 1.665 MeV and the n-α-α threshold at 1.573 MeV provided a vanishing cross section ($9.3 \times 10^{-5} \pm 0.016$ mb) at 1.63 MeV.

The data measured from the n-^{8}Be threshold to 1.78 MeV were fitted with the Breit-Wigner (B-W) function with a focus on the low-energy behavior of the cross section:

$$\sigma(E_\gamma) = \pi \left(\frac{\hbar c}{E_\gamma}\right)^2 \frac{\Gamma_\gamma \Gamma_n}{(E_\gamma - E_R)^2 + (\Gamma/2)^2}. \qquad (7)$$

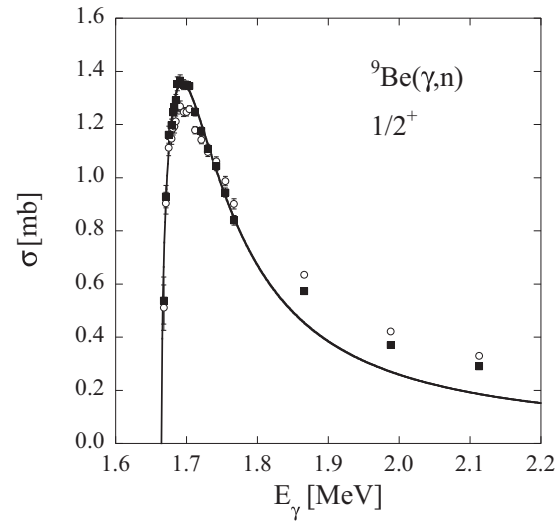

FIG. 10. The present ^{9}Be(γ,n) cross section corrected for the energy spread of the LCS γ-ray beam is shown by the solid squares and the monochromatic cross section is shown by the open circles. The solid line represents the Breit-Wigner fit to the cross section.

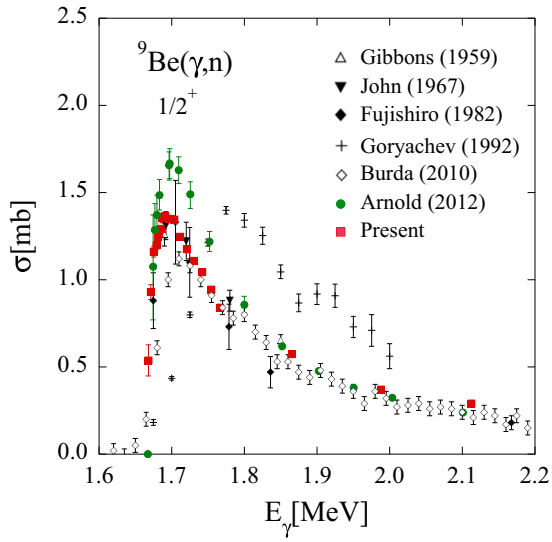

FIG. 11. (Color online) The present ^{9}Be(γ,n) cross section in comparison with the existing data (filled circles: Ref. [6], filled diamonds: Ref. [42], inverted filled triangles: Ref. [40], open triangles: Ref. [41], crosses: Ref. [16], open diamonds: Ref. [38]).

The γ width Γ_γ is related to the reduced transition probability $B(E1)\downarrow$ [35] by

$$\Gamma_\gamma = \frac{16\pi}{9}\alpha(\hbar c)^{-2}E_\gamma^3 B(E1)\downarrow. \quad (8)$$

The neutron width Γ_n for s-wave neutrons from the $1/2^+$ state was taken [36] as

$$\Gamma_n = 2\sqrt{\epsilon_R(E_\gamma - S_n)}. \quad (9)$$

The threshold cross section is well fitted with the B-W function as shown by the solid line. The B-W fit, however, underestimates the experimental data measured above 1.8 MeV. This underestimate may be associated with the onset of the three-body breakup in this energy region as indicated by the mean neutron energies.

The best-fit resonance parameters are listed in Table I, in comparison with those of Refs. [5,6]. The present result is consistent with the 2001 data [5]. It is to be noted that the disagreement in $B(E1)$ between the (γ, n) [5,37] and (e, e') [38,39] data was recently analyzed and resolved as a way of integration of the resonance [12].

The threshold behavior of the present cross section is shown in Fig. 11 in comparison with the existing data including those taken with radioactive isotopes [40–42] and bremsstrahlung [16]. The deconvoluted cross section of the 2012 data (Fig. 7 of Ref. [6]) is shown in the figure. Note that the 2012 data give a peak cross section (∼1.7 mb) that is much higher than that (1.35 mb) of the present data. The data of the radioactive isotope measurements are rather consistent with the present data, while the bremsstrahlung data exhibit a very different threshold behavior. Averaged photoneutron cross sections extracted from the (e, e') data [38,43] are also shown in the figure.

We remark that the B-W fit may not serve as evidence that the $1/2^+$ state is a resonant state though the energy and width parameters resulting from the R-matrix analysis are also consistent with the resonance nature of the $1/2^+$ state [12]. A similar threshold behavior of the cross section may arise from a virtual state in the potential model of n-^{8}Be scattering [13] and the complex scaling method of describing the n-α-α system [15]. The authors were informed in private communication that the present cross section is reproduced by the complex scaling method [44].

C. Cluster dipole resonance

A significant resonance was confirmed in the present measurement in the energy region immediately below GDR as shown in Fig. 12. The present data (filled squares) show even more enhanced cross sections than the bremsstrahlung data (crosses) at energies higher than 8 MeV. The cluster dipole resonance has a significant strength compared to the observed GDR. In the figure, the GDR data (open circles) are a sum of (γ, n), (γ, $n+p$), (γ, $2n$), and (γ, $2n+p$) cross sections of Ref. [45]. The 2001 data [5] (filled circles) are shown for the $5/2^+$ state. For the $1/2^+$ state, the present data as well as the deconvoluted cross section of Ref. [6] (filled diamonds) and the bremsstrahlung data of Ref. [16] (crosses) are shown.

The CDR strength was deduced by a global fit to the data of GDR [45], CDR, and the $5/2^+$ state [5] with the least-squares method. The Lorentzian and B-W functions were used for the GDR and the $5/2^+$ state, respectively, while the Gaussian function was used for CDR assuming that its strength is localized in the low-energy tail of the GDR. The best-fit function is shown by the dot-dashed line in Fig. 12 along with its breakdown to the GDR, CDR, and $5/2^+$ state by the dashed, solid, dotted lines, respectively. The energy-integrated strength of the CDR is 11.3 mb MeV.

We remark that the resonance strength depends on the shape of the low-energy tail of the GDR which is estimated by the Lorentzian function. The value (11.3 mb MeV) may represent a lower limit because it is known that the Lorentzian type of the γ-ray strength function (photoabsorption cross section) significantly overestimates (n, γ) cross sections for

TABLE I. Resonance parameters obtained in the Breit-Wiger fit to the (γ, n) cross section data for the $1/2^+$ state.

E_R (MeV)	Γ_n (keV)	Γ_γ (eV)	$B(E1)\downarrow$ (e^2 fm^2)	Ref.
1.748 ± 0.01	283 ± 42	0.598 ± 0.004	0.107 ± 0.007	Utsunomiya *et al.* [5]
1.735 ± 0.003	225 ± 12	0.568 ± 0.001	0.104 ± 0.002	Sumiyoshi *et al.* [37]
1.731 ± 0.002	213 ± 6	0.738 ± 0.002	0.136 ± 0.002	Arnold *et al.* [6]
1.728 ± 0.001	214 ± 7	0.595 ± 0.002	0.111 ± 0.004	Present

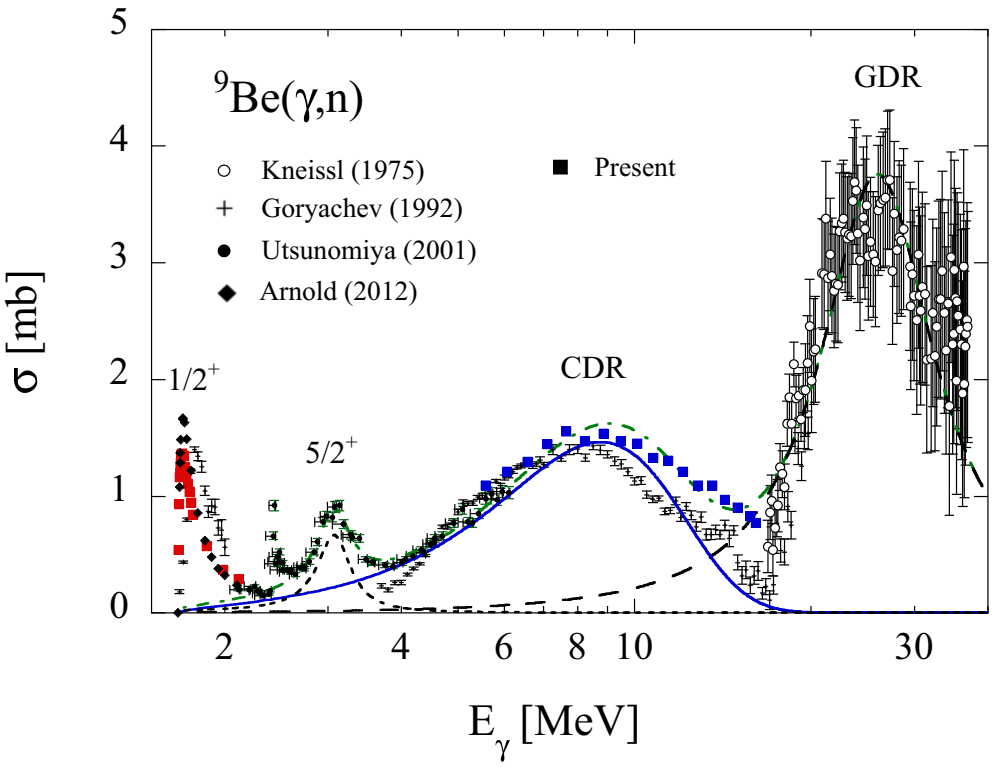

FIG. 12. (Color online) The ^{9}Be(γ,n) cross section in the energy region from the $n + {}^8$Be threshold to GDR (see text for details).

heavy nuclei [46–49]. The strength integrated over 4–16 MeV without a contribution from the low-energy tail of the GDR is 14.2 mb MeV. Thus, the resonance strength is 11.3–14.2 mb MeV.

Let us compare the resonance strength with the cluster dipole sum rule [50–52] for the two-body (n-^{8}Be) and three-body (n-α-α) systems:

$$\int \sigma_{E1}(E)dE = 60\left(\frac{NZ}{A} - \sum_i \frac{N_i Z_i}{A_i}\right). \qquad (10)$$

The first term of Eq. (10) is the Thomas-Reiche-Kuhn (TRK) sum rule representing the $E1$ response of a nucleus in the absence of exchange forces. After subtracting the intrinsic contributions from the constituent clusters from the entire response, the sum rule represents the $E1$ response arising from relative motions between the constituents. The cluster dipole sum rule gives 10% (13.3 mb MeV) of the TRK sum rule (133 mb MeV), irrespective of the two-body (n-^{8}Be) or three-body (n-α-α) systems. The present strength is consistent with the cluster dipole sum rule, which however does not distinguish whether a neutron oscillates in the n-^{8}Be or n-α-α configuration. It is desirable to investigate the nature of the cluster dipole resonance both experimentally and theoretically. The investigation requires a new experiment of n-α-α coincidences to measure correlations of a neutron against two α particles. The authors are informed in private communication that a theoretical investigation is in progress based on the antisymmetrized molecular dynamics calculation [53].

V. CONCLUSIONS

The photodisintegration of ^{9}Be through the $1/2^+$ state and cluster dipole resonance was measured. The cross section of the $1/2^+$ state is consistent with the 2001 data and the data of the radioactive isotope measurements. The observed resonance strength is consistent with the cluster dipole sum rule. However, the sum rule degenerates in the two-body (n-^{8}Be) and three-body (n-α-α) systems. Consequently, the present result does not distinguish whether a neutron oscillates in the two-body or three-body configuration. A new n-α-α coincidence experiment is needed to investigate the configuration. A theoretical study is encouraged to investigate the nature of the $1/2^+$ state and the nuclear structure of the cluster dipole resonance in ^{9}Be.

ACKNOWLEDGMENTS

We are indebted to Masayasu Kamimura of RIKEN for drawing our attention to the stau-catalyzed big-bang nucleosynthesis and Kiyoshi Kato of Hokkaido University for discussions on resonant and virtual states. We thank Akinori Takemoto and Masashi Yamaguchi for their assistance in tuning the CO_2 laser and the double collimators for producing low-energy LCS γ-ray beams. This work was supported by the Japan Private School Promotion Foundation. I.G. acknowledges financial support from the Extreme Light Infrastructure Nuclear Physics (ELI-NP) Phase I, a project cofinanced by the Romanian Government and the European Union through the European Regional Development Fund (425/12.12.2012, POS CCE, ID 1334 SMIS-CSNR 40741).

[1] T. Sasaqui, K. T. Kajino, G. Mathews, K. Otsuki, and T. Nakamura, Astrophys. J. **634**, 1173 (2005).
[2] S. E. Woosley, J. R. Wilson, G. J. Mathews, R. D. Hoffmman, and B. S. Meyer, Astrophys. J. **433**, 229 (1994).
[3] C. Freburghaus, S. Rosswog, and F.-K. Thielemann, Astrophys. J. **525**, L121 (1999).
[4] M. Terasawa, K. Sumiyoahi, T. Kajino, G. Mathews, and I. Tanihata, Astrophys. J. **562**, 470 (2001).
[5] H. Utsunomiya, Y. Yonezawa, H. Akimune, T. Yamagata, M. Ohta, M. Fujishiro, H. Toyokawa, and H. Ohgaki, Phys. Rev. C **63**, 018801 (2000).
[6] C. W. Arnold, T. B. Clegg, C. Iliadis, H. J. Karwowski, G. C. Rich, J. R. Tompkins, and C. R. Howell, Phys. Rev. C **85**, 044605 (2012).
[7] M. Pospelov, J. Pradler, and F. D. Steffen, J. Cosmol. Astropart. Phys. **11**, 020 (2008).
[8] F. Iocco, G. Mangano, G. Miele, O. Pisanti, and P. D. Serpico, Phys. Rep. **472**, 1 (2009).
[9] M. Kamimura, Y. Kino, and E. Hiyama, Prog. Theor. Phys. **121**, 1059 (2009).
[10] E. Garrido, D. V. Fedorov, and A. S. Jense, Phys. Lett. B **684**, 132 (2010).
[11] R. Álvarez-Rodríguez, A. S. Jensen, E. Garrido, and D. V. Fedorov, Phys. Rev. C **82**, 034001 (2010).
[12] V. D. Efros, P. von Neumann-Cosel, and A. Richter, Phys. Rev. C **89**, 027301 (2014).
[13] V. D. Efros and J. M. Bang, Eur. Phys. J. A **4**, 33 (1999).
[14] K. Arai, P. Descouvemont, D. Baye, and W. N. Catford, Phys. Rev. C **68**, 014310 (2003).
[15] M. Odsuren, Y. Kikuchi, T. Myo, M. Aikawa, and K. Kato, Phys. Rev. C **92**, 014322 (2015).
[16] A. M. Goryachev, G. N. Zalesnyy, and I. V. Pozdnev, Izv. Ross. Akad. Nauk, Ser. Fiz. **56**, 159 (1992).
[17] S. Amano, K. Horikawa, K. Ishihara, S. Miyamoto, T. Hayakawa, T. Shizuma, and T. Mochizuki, Nucl. Instrum. Methods Phys. Res. A **602**, 337 (2009).
[18] S. Agostinelli *et al.*, Nucl. Instrum. Methods Phys. Res. A **506**, 250 (2003).
[19] H. Utsunomiya *et al.*, IEEE Trans. Nucl. Sci. **61**, 1252 (2014).
[20] T. Kii *et al.*, in *Proceedings of the 12th Symposium on Accelerator Science and Technology*, edited by Yasushige Yano (The Institute of Physical and Chemical Research (RIKEN), Wako, Japan, 1999), pp. 484–485.
[21] H. Toyokawa, T. Kii, H. Ohgaki, T. Shima, T. Baba, and Y. Nagai, IEEE Trans. Nucl. Sci. **47**, 1954 (2000).
[22] T. Kondo *et al.*, Nucl. Instrum. Methods Phy. Res. A **659**, 462 (2011).
[23] J. F. Briesmeister, computer code MCNP, Version 4C (Los Alamos National Laboratory, Los Alamos, 2000).
[24] D. M. Filipescu, I. Gheorghe, H. Utsunomiya, S. Goriely, T. Renstrom, H. T. Nyhus, O. Tesileanu, T. Glodariu, T. Shima, K. Takahisa, S. Miyamoto, Y. W. Lui, S. Hilaire, S. Peru, M. Martini, and A. J. Koning, Phys. Rev. C **90**, 064616 (2014).
[25] H. T. Nyhus, T. Renstrom, H. Utsunomiya, S. Goriely, D. M. Filipescu, I. Gheorghe, O. Tesileanu, T. Glodariu, T. Shima, K. Takahisa, S. Miyamoto, Y. W. Lui, S. Hilaire, S. Peru, M. Martini, L. Siess, and A. J. Koning, Phys. Rev. C **91**, 015808 (2015).
[26] B. L. Berman, R. E. Pywell, S. S. Dietrich, M. N. Thompson, K. G. McNeill, and J. W. Jury, Phys. Rev. C **36**, 1286 (1987).
[27] O. Itoh *et al.*, J. Nucl. Sci. Technol. **48**, 834 (2011).
[28] J. Ahrens *et al.*, Phys. Lett. B **52**, 49 (1974).
[29] Y. Birenbaum, S. Kahane, and R. Moreh, Phys. Rev. C **32**, 1825 (1985).
[30] R. Bernabei, A. Chisholm, S. dAngelo, M. P. DePascale, P. Picozza, C. Schaerf, P. Belli, L. Casano, A. Incicchitti, D. Prosperi, and B. Girolami, Phys. Rev. C **38**, 1990 (1988).
[31] R. Moreh, T. J. Kennett, and W. V. Prestwich, Phys. Rev. C **39**, 1247 (1989).
[32] K. Y. Hara, H. Utsunomiya, S. Goko, H. Akimune, T. Yamagata, M. Ohta, H. Toyokawa, K. Kudo, A. Uritani, Y. Shibata, Y. W. Lui, and H. Ohgaki, Phys. Rev. D **68**, 072001 (2003).
[33] http://wwwndc.jaea.go.jp/jendl/j40/J40_J.html.
[34] https://www-nds.iaea.org/exfor/exfor.htm.
[35] J. M. Blatt and V. F. Weisskopf, *Theoretical Nuclear Physics* (Springer-Verlag, New York, 1952), p. 583.
[36] E. Wigner, Phys. Rev. **73**, 1002 (1948).
[37] K. Sumiyoshi, H. Utsunomiya, S. Goko, and T. Kajino, Nucl. Phys. A **709**, 467 (2002).
[38] O. Burda, P. von Neumann-Cosel, A. Richter, C. Forssén, and B. A. Brown, Phys. Rev. C **82**, 015808 (2010).
[39] J. P. Glickman, W. Bertozzi, T. N. Buti, S. Dixit, F. W. Hersman, C. E. Hyde-Wright, M. V. Hynes, R. W. Lourie, B. E. Norum, J. J. Kelly, B. L. Berman, and D. J. Millener, Phys. Rev. C **43**, 1740 (1991).
[40] J. H. Gibbons *et al.*, Phys. Rev. **114**, 1319 (1959).
[41] W. John and J. M. Prosser, Phys. Rev. **163**, 958 (1967).
[42] M. Fujishiro *et al.*, Can. J. Phys. **60**, 1672 (1982); **61**, 1579 (1983).
[43] G. Kuechler, A. Richter, and W. von Witsch, Z. Phys. A **326**, 447 (1987).
[44] Y. Kikuchi (private communication).
[45] U. Kneissl, G. Kuhl, K.-H. Leister, and A. Weller, Nucl. Phys. A **247**, 91 (1975).
[46] H. Utsunomiya, S. Goriely, M. Kamata, T. Kondo, O. Itoh, H. Akimune, T. Yamagata, H. Toyokawa, Y. W. Lui, S. Hilaire, and A. J. Koning, Phys. Rev. C **80**, 055806 (2009).
[47] H. Utsunomiya, S. Goriely, H. Akimune, H. Harada, F. Kitatani, S. Goko, H. Toyokawa, K. Yamada, T. Kondo, O. Itoh, M. Kamata, T. Yamagata, Y. W. Lui, S. Hilaire, and A. J. Koning, Phys. Rev. C **81**, 035801 (2010).
[48] H. Utsunomiya, S. Goriely, H. Akimune, H. Harada, F. Kitatani, S. Goko, H. Toyokawa, K. Yamada, T. Kondo, O. Itoh, M. Kamata, T. Yamagata, Y. W. Lui, I. Daoutidis, D. P. Arteaga, S. Hilaire, and A. J. Koning, Phys. Rev. C **82**, 064610 (2010).
[49] H. Utsunomiya, S. Goriely, M. Kamata, H. Akimune, T. Kondo, O. Itoh, C. Iwamoto, T. Yamagata, H. Toyokawa, Y. W. Lui, H. Harada, F. Kitatani, S. Goko, S. Hilaire, and A. J. Koning, Phys. Rev. C **84**, 055805 (2011).
[50] Y. Alhassid, M. Gai, and G. F. Bertsch, Phys. Rev. Lett. **49**, 1482 (1982).
[51] H. Sagawa and M. Honma, Phys. Lett. B **251**, 17 (1990).
[52] R. deDiego, E. Garrido, A. S. Jensen, and D. V. Fedorov, Phys. Rev. C **77**, 024001 (2008).
[53] Y. Kanada-En'yo (private communication).